Eur. Phys. J. A **17**, 475–481 (2003)
DOI 10.1140/epja/i2002-10195-4

THE EUROPEAN PHYSICAL JOURNAL A

Neutrino interactions in dense stellar matter

S. Reddy[a]

Center for Theoretical Physics, Massachusetts Institute of Technology, 77 Mass. Ave, Cambridge MA 02139, USA and Los Alamos National Laboratory, P.O. Box 1663, MS B283, Los Alamos, NM 87545, USA[b]

Received: 1 November 2002 /
Published online: 15 July 2003 – © Società Italiana di Fisica / Springer-Verlag 2003

Abstract. Weak-interaction rates play an important role in the birth of neutron stars in core collapse supernova and their subsequent thermal evolution. In this paper, I highlight the role of strong interactions and phase transitions in calculations of neutrino scattering and emission rates in dense stellar matter.

PACS. 13.15.+g Neutrino interactions – 13.20.-v Leptonic and semileptonic decays of mesons – 26.50.+x Nuclear physics aspects of novae, supernovae, and other explosive environments – 26.60.+c Nuclear matter aspects of neutron stars

1 Introduction

Neutrinos play an important role in stellar evolution. By virtue of their weak interactions with matter, neutrinos provide a mechanism for energy loss from the dense stellar interiors. In neutron stars neutrinos are responsible for most of the energy radiated from the their birth in a supernova explosion until several thousand years of subsequent evolution. In this paper, we present an overview of some of the nuclear/particle physics issues that play a role in understanding the rate of propagation and production of neutrinos inside neutron stars. The calculation of these rates are of current interest since several research groups are embarking on large-scale numerical simulations of supernova and neutron star evolution. Even moderate changes in the nuclear microphysics associated with the weak-interaction rates at high density can impact macroscopic features that are observable. An understanding of the response of strongly interacting nuclear medium to neutrinos and its impact on neutron star evolution, promises to provide a means to probe the properties of the dense medium itself.

This paper covers two related topics: i) neutrino interactions in dense matter containing nucleons and leptons and ii) neutrino interactions in exotic new phases that are likely to occur in the dense inner core of the neutron star. We emphasize the generic aspects of the microphysics that affects the weak-interaction rates and present supporting qualitative arguments. (For a detailed account see ref. [1].)

[a] e-mail: reddy@lanl.gov
[b] *Present address.*

2 Neutrino interactions in nucleonic matter

It was realized over a decade ago that the effects due to degeneracy and strong interactions significantly alter the neutrino mean free paths and neutrino emissivities in dense matter [2–5]; it is only recently that detailed calculations have become available [6–16]. The scattering and absorption reactions that contribute to the neutrino opacity are

$$\nu_e + B \to e^- + B' , \qquad \bar{\nu}_e + B \to e^+ + B' ,$$
$$\nu_X + B \to \nu_X + B' , \qquad \nu_X + e^- \to \nu_X + e^- ,$$

where the scattering reactions are common to all neutrino species and the dominant source of opacity for the electron neutrinos is due to the charged reaction. The important neutrino-producing reactions in the neutron star context are

$$e^- + p \to n + \nu_e , \qquad n \to e^- + p + \bar{\nu}_e ,$$
$$n + n \to n + p + e^- + \bar{\nu}_e , \qquad n + n \to n + n + \nu_X + \bar{\nu}_X$$

The weak-interaction rates in hot and dense matter are modified due to many in-medium effects. The most important of these are:

1) *Composition*: The rate for neutrino processes depend sensitively on the composition which is sensitive to the nature of strong interactions. First, the different degeneracies of the different fermions determine the single-pair response due to Pauli blocking. For example, a larger symmetry energy favors higher proton fractions. This directly impacts the weak rates since the Second neutrinos couple differently to different baryonic species; consequently, the net rates will depend on the individual concentrations.

2) *In-medium dispersion relations*: At high density, the single-particle spectra are significantly modified from their non-interacting forms due to effects of strong interactions. Interacting matter features smaller effective baryon masses and energy shifts relative to non-interacting matter. This in turn affects the weak-interaction rates primarily because it modifies the density of particle-hole states at the Fermi surface.
3) *Correlations*: Low-energy neutrinos couple mainly to the long-wavelength fluctuations of the strongly interacting nuclear plasma. Repulsive particle-hole interactions and Coulomb interactions generally result in a suppression of the weak-interaction rates since they increase the energy cost associated with such fluctuations. Interactions can also result in low-lying collective excitations to which neutrinos can couple. This acts to increase the weak-interaction rates at low energy. Both effects may be calculated using the Random-Phase Approximation (RPA), in which ring diagrams are summed to all orders. Model calculations [2,5,4,6,9,11,13–15] indicate that at high density the neutrino cross-sections are suppressed relative to the case in which these effects are ignored. In addition, these correlations enhance the average energy transfer in neutrino-nucleon collisions. Improvements in determining the many-body dynamic form factor and assessing the role of particle-particle interactions in dense matter at finite temperature are necessary before the full effects of many-body correlations may be ascertained.

The relative importance of the various effects described above on neutrino transport is only beginning to be studied systematically. As a first step, we will focus on effects due to modifications 1) through 3) above. To see how this is accomplished, we start with a general expression for the differential cross-section [6,13]:

$$\frac{1}{V}\frac{\mathrm{d}^3\sigma}{\mathrm{d}^2\Omega_3\mathrm{d}E_3} = -\frac{G_F^2}{128\pi^2}\frac{E_3}{E_1}\left[1-\exp\left(\frac{-q_0-(\mu_2-\mu_4)}{T}\right)\right]^{-1} \times(1-f_3(E_3))\mathrm{Im}(L^{\alpha\beta}\Pi^R_{\alpha\beta})\,, \quad (1)$$

where the incoming-neutrino energy is E_1 and the outgoing-electron energy is E_3. The factor $[1-\exp((-q_0-\mu_2+\mu_4)/T)]^{-1}$ maintains detailed balance, for particles labeled "2" and "4" which are in thermal equilibrium at temperature T and in chemical equilibrium with chemical potentials μ_2 and μ_4, respectively. The final-state blocking of the outgoing lepton is accounted for by the Pauli-blocking factor $(1-f_3(E_3))$. The lepton tensor $L_{\alpha\beta}$ is given by

$$L^{\alpha\beta} = 8[2k^\alpha k^\beta + (k\cdot q)g^{\alpha\beta} - (k^\alpha q^\beta + q^\alpha k^\beta) \mp i\epsilon^{\alpha\beta\mu\nu}k^\mu q^\nu]. \quad (2)$$

The target particle retarded polarization tensor is

$$\mathrm{Im}\Pi^R_{\alpha\beta} = \tanh\left(\frac{q_0+(\mu_2-\mu_4)}{2T}\right)\mathrm{Im}\ \Pi_{\alpha\beta}\,, \quad (3)$$

where $\Pi_{\alpha\beta}$ is the time ordered or causal polarization and is given by

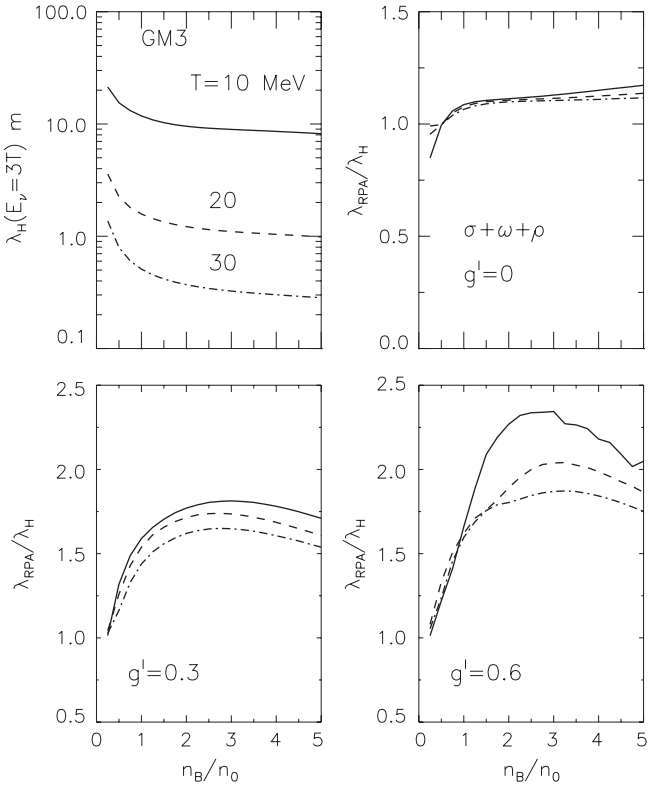

Fig. 1. Neutrino mean free paths in relativistic RPA.

$$\Pi_{\alpha\beta} = -i\int\frac{\mathrm{d}^4p}{(2\pi)^4}\mathrm{Tr}\ [T(G_2(p)J_\alpha G_4(p+q)J_\beta)]\,. \quad (4)$$

Above, k_μ is the incoming-neutrino four-momentum and q_μ is the four-momentum transfer. In writing the lepton tensor, we have neglected the electron mass term, since typical electron energies are of the order of a few hundred MeV. The Greens' functions $G_i(p)$ (the index i labels particle species) describe the propagation of baryons at finite density and temperature. The current operator J_μ is γ_μ for the vector current and $\gamma_\mu\gamma_5$ for the axial current. Effects of strong and electromagnetic correlations may be calculated by utilizing the RPA polarization tensor

$$\Pi^{\mathrm{RPA}} = \Pi + \Pi^{\mathrm{RPA}}D\Pi\,, \quad (5)$$

where D denotes the interaction matrix, in eq. (1) (see [13] for more details).

Neutrino mean free paths calculated in relativistic RPA are shown in fig. 1. The model employed incorporates interactions via σ-ω-ρ exchange as in Walecka model. It is supplemented by pion exchange and a repulsive contact term whose strength is parameterized by the constant g' to account for short range spin-isospin correlations. The results indicate that RPA corrections are most significant in the spin-isospin channel and that low-temperature correlation can suppress the cross-section by as much as a factor of 2-3. Quantitative aspects of the suppression depends on the details of the model employed, nonetheless we note that most model studies thus far indicate similar suppression factors.

3 Neutrino interactions in novel phases at high density

In this section we explore how phase transitions impact the weak-interaction rates. Novel phases of baryonic matter are expected to occur at densities accessible in neutron stars. These new phases include pion condensation, kaon condensation, hyperons and quark matter. An understanding of how these phases might influence neutrino propagation and emission is necessary if we are to inquire if these phase transitions even occur in side neutron stars. We consider three specific examples of phase transitions: i) generic first-order transitions; 2) superconducting quark matter and 3) Color-Flavor–Locked superconducting quark matter to explore and illustrate the modification of neutrino rates in the novel high-density phases of matter.

3.1 Inhomogeneous phases: effects of first-order transitions

First-order phase transitions in neutron stars can result in the formation of heterogeneous phases in which a positively charged nuclear phase coexists with a negatively charged new phase which is favored at higher densities [17]. This is a generic feature of first-order transitions in matter with two conserved charges. In the neutron star context these correspond to baryon number and electric charge. Reddy, Bertsch and Prakash [18] have studied the effects of inhomogeneous phases on ν-matter interactions. Based on simple estimates of the surface tension between nuclear matter and the exotic phase, typical droplet sizes range from 5 to 15 fm [19], and inter-droplet spacings range up to several times larger. The propagation of neutrinos whose wavelength is greater than the typical droplet size and less than the inter-droplet spacing, *i.e.*, 2 MeV $\leq E_\nu \leq$ 40 MeV, will be greatly affected by the heterogeneity of the mixed phase, as a consequence of the coherent scattering of neutrinos from the matter in the droplet.

The Lagrangian that describes the neutral current coupling of neutrinos to the droplet is

$$\mathcal{L}_W = \frac{G_F}{2\sqrt{2}}\ \bar{\nu}\gamma_\mu(1-\gamma_5)\nu\ J_D^\mu\,, \tag{6}$$

where J_D^μ is the neutral current carried by the droplet and $G_F = 1.166\times10^{-5}$ GeV^{-2} is the Fermi weak-coupling constant. For non-relativistic droplets, $J_D^\mu = \rho_W(x)\delta^{\mu 0}$ has only a time-like component. Here, $\rho_W(x)$ is the excess weak charge density in the droplet. The total weak charge enclosed in a droplet of radius r_d is $N_W = \int_0^{r_d} \mathrm{d}^3x\rho_W(x)$ and the form factor is $F(q) = (1/N_W)\int_0^{r_d}\mathrm{d}^3x\rho_W(x)\sin qx/qx$. The differential cross-section for neutrinos scattering from an isolated droplet is then

$$\frac{\mathrm{d}\sigma}{\mathrm{d}\cos\theta} = \frac{E_\nu^2}{16\pi}G_F^2N_W^2(1+\cos\theta)F^2(q)\,. \tag{7}$$

In the above equation, E_ν is the neutrino energy and θ is the scattering angle. Since the droplets are massive, we consider only elastic scattering for which the magnitude of the momentum transfer is $q=\sqrt{2}E_\nu(1-\cos\theta)$.

We must embed the droplets into the medium to evaluate the neutrino transport parameters. The droplet radius r_d and the inter-droplet spacing are determined by the interplay of surface and Coulomb energies. In the Wigner-Seitz approximation, the cell radius is $R_W = (3/4\pi N_D)^{1/3}$ where the droplet density is N_D. Multiple droplet scattering cannot be neglected for $E_\nu \lesssim 1/R_W$. The effects of other droplets is to cancel scattering in the forward direction, because the interference is destructive except at exactly zero degrees, where it produces a change in the index of refraction of the medium. These effects are usually incorporated by multiplying the differential cross-section, eq. (7), by the static form factor of the medium. The static form factor, defined in terms of the radial distribution function of the droplets, $g(r)$, is

$$S(q) = 1 + N_D\int \mathrm{d}^3r\exp i\mathbf{q}\cdot\mathbf{r}\ (g(r)-1)\,. \tag{8}$$

The droplet correlations, which determine $g(r)$, arise due to the Coulomb force and are measured in terms of the dimensionless Coulomb number $\Gamma = Z^2e^2/(8\pi R_W kT)$. Due to the long-range character of the Coulomb force, the role of screening and the finite droplet size, $g(r)$ cannot be computed analytically. We use a simple ansatz for the radial distribution function $g(r<R_W)=0$ and $g(r>R_W)=1$. The simple ansatz for $g(r)$ is equivalent to subtracting, from the weak charge density ρ_W, a uniform density which has the same total weak charge N_W as the matter in the Wigner-Seitz cell. Thus, effects due to $S(q)$ may be incorporated by replacing the form factor $F(q)$ by

$$F(q)\to\tilde{F}(q) = F(q) - 3\ \frac{\sin qR_W - (qR_W)\cos qR_W}{(qR_W)^3}\,. \tag{9}$$

The neutrino-droplet differential cross-section per unit volume then follows:

$$\frac{1}{V}\frac{\mathrm{d}\sigma}{\mathrm{d}\cos\theta} = N_D\ \frac{E_\nu^2}{16\pi}G_F^2N_W^2(1+\cos\theta)\tilde{F}^2(q)\,. \tag{10}$$

Note that even for small droplet density N_D, the factor N_W^2 acts to enhance the droplet scattering. To quantify the importance of droplets as a source of opacity, we compare with the standard scenario in which matter is uniform and composed of neutrons. The dominant source of opacity is then due to scattering from thermal fluctuations and

$$\frac{1}{V}\frac{\mathrm{d}\sigma}{\mathrm{d}\cos\theta} = \frac{G_F^2}{8\pi}\left(c_V^2(1+\cos\theta)+(3-\cos\theta)c_A^2\right)\ E_\nu^2 \times\frac{3}{2}\ n_n\ \left[\frac{k_BT}{E_{Fn}}\right]\,, \tag{11}$$

where c_V and c_A are, respectively, the vector and axial coupling constants of the neutron, n_n is the neutron number density, E_{Fn} is the neutron Fermi energy and T is the matter temperature [4].

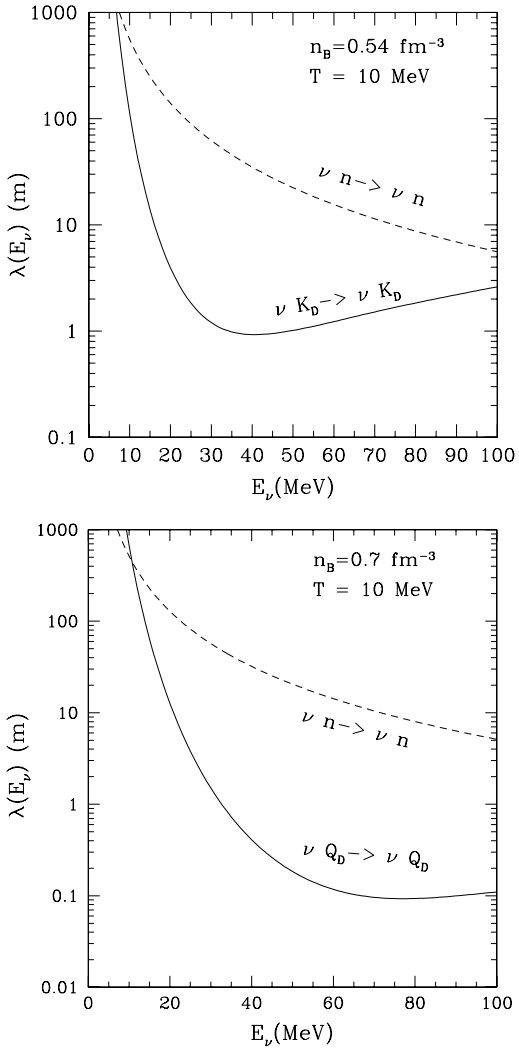

Fig. 2. Neutrino mean free paths as a function of neutrino energy. Solid lines are for matter in a mixed phase containing kaons (upper panel) and quarks (lower panel), and dashed curves are for uniform matter.

The transport cross-sections that are employed in studying the diffusive transport of neutrinos in the core of a neutron star are differential cross-sections weighted by the angular factor $(1-\cos\theta)$. The transport mean free path $\lambda(E_\nu)$ for a given neutrino energy E_ν is given by

$$\frac{1}{\lambda(E_\nu)} = \frac{\sigma_T(E_\nu)}{V} = \int \mathrm{d}\cos\theta (1-\cos\theta) \left[\frac{1}{V}\frac{\mathrm{d}\sigma}{\mathrm{d}\cos\theta}\right]. \quad (12)$$

Models of first-order phase transitions in dense matter provide the weak charge and form factors of the droplets and permit the evaluation of ν-droplet scattering contributions to the opacity of the mixed phase. We consider two models, namely the first-order kaon condensate and the quark-hadron phase transition; the neutrino mean free paths in the mixed phase are shown in the upper and lower panels of fig. 2, respectively. The results are shown for the indicated values of the baryon density n_B and temperature T where the model predicts a mixed phase exists. The kaon droplets are characterized by radii $r_d \sim 7$ fm and inter-droplet spacings $R_W \sim 20$ fm, and enclose a net weak vector charge $N_W \sim 700$. The quark droplets are characterized by $r_d \sim 5$ fm and $R_W \sim 11$ fm, and an enclosed weak charge $N_W \sim 850$. For comparison, the neutrino mean free paths in uniform neutron matter at the same n_B and T are also shown. It is apparent that there is a large coherent scattering-induced reduction in the mean free path for the typical energy $E_\nu \sim \pi T$. At much lower energies, the inter-droplet correlations tend to screen the weak charge of the droplet, and at higher energies the coherence is attenuated by the droplet form factor.

The large reduction in neutrino mean free path found here implies that the mixed phase will cool significantly slower than homogeneous matter. Consequently, the observable neutrino luminosity at late times might be affected as it is driven by the transport of energy from the deep interior.

3.2 Effects of quark superconductivity

Recent theoretical works [20,21] suggest that quarks form Cooper pairs in medium, a natural consequence of attractive interactions destabilizing the Fermi surface. Although the idea of quark pairing in dense matter is not new [20], it has recently seen renewed interest in the context of the phase diagram of QCD [21]. Model calculations, mostly based on four-quark effective interactions, predict the restoration of spontaneously broken chiral symmetry through the onset of color superconductivity at low temperatures. They predict an energy gap of $\Delta \sim 100$ MeV for a typical quark chemical potential of $\mu_q \sim 400$ MeV. As in BCS theory, the gap will weaken for $T > 0$, and at some critical temperature T_c there is a (second-order) transition to a "standard" quark-gluon plasma. During cooling from an initial temperature in excess of T_c, the formation of a gap in the fermionic excitation spectrum in quark matter will influence various transport properties of the system. Carter and Reddy have studied its influence on the transport of neutrinos [22].

The differential neutrino scattering cross-section per unit volume in an infinite and homogeneous system of relativistic fermions as calculated in linear-response theory is given by eq. (1). The medium is characterized by the quark polarization tensor $\Pi_{\alpha\beta}$. In the case of free quarks, each flavor contributes a term of the form

$$\Pi_{\alpha\beta}(q) = -i\mathrm{Tr}_c \int \frac{\mathrm{d}^4p}{(2\pi)^4} \mathrm{Tr}\left[S_0(p)\Gamma_\alpha S_0(p+q)\Gamma_\beta\right], \quad (13)$$

where $S_0(p)$ is the free quark propagator at finite chemical potential and temperature. The outer trace is over color and simplifies to a $N_c = 3$ degeneracy. The inner trace is over spin, and the Γ_α are the neutrino-quark vertex functions which determine the spin channel. Specifically, the vector polarization is computed by choosing $(\Gamma_\alpha, \Gamma_\beta) = (\gamma_\alpha, \gamma_\beta)$. The axial and mixed vector-axial polarizations are similarly obtained from $(\Gamma_\alpha, \Gamma_\beta) = (\gamma_\alpha\gamma_5, \gamma_\beta\gamma_5)$ and $(\Gamma_\alpha, \Gamma_\beta) = (\gamma_\alpha, \gamma_\beta\gamma_5)$, respectively.

The free quark propagators in eq. (13) are naturally modified in a superconducting medium. As first pointed out by Bardeen, Cooper, and Schrieffer several decades ago, the quasi-particle dispersion relation is modified due to the presence of a gap in the excitation spectrum. In calculating these effects, we will consider the simplified case of QCD with two quark flavors which obey $SU(2)_L \times SU(2)_R$ flavor symmetry, given that the light u- and d-quarks dominate low-energy phenomena. Furthermore, we will assume that, through some unspecified effective interactions, quarks pair in a manner analogous to the BCS mechanism [23]. The relevant consequences of this are the restoration of chiral symmetry (hence all quarks are approximately massless) and the existence of an energy gap at zero temperature, Δ_0, with approximate temperature dependence,

$$\Delta(T) = \Delta_0 \sqrt{1 - \left(\frac{T}{T_c}\right)^2}\,. \tag{14}$$

The critical temperature $T_c \simeq 0.57\Delta_0$ is likewise taken from BCS theory; this relation has been shown to hold for perturbative QCD and is thus a reasonable assumption for non-perturbative physics. Since the scalar diquark (in the $\bar{\mathbf{3}}$-color representation) appears to always be the most attractive channel, we consider the anomalous (or Gorkov) propagator [24]

$$\begin{aligned} F(p)_{abfg} &= \langle q^T_{fa}(p) C\gamma_5 q_{gb}(-p)\rangle \\ &= -i\epsilon_{ab3}\epsilon_{fg}\Delta \left(\frac{\Lambda^+(p)}{p_o^2 - \xi_p^2} + \frac{\Lambda^-(p)}{p_o^2 - \bar{\xi}_p^2}\right)\gamma_5 C\,. \end{aligned} \tag{15}$$

Here, a, b are color indices, f, g are flavor indices, ϵ_{abc} is the usual anti-symmetric tensor and we have conventionally chosen 3 to be the condensate color. This propagator is also anti-symmetric in flavor and spin, with $C = -i\gamma_0\gamma_2$ being the charge conjugation operator. The color bias of the condensate forces a splitting of the normal quark propagator into colors transverse and parallel to the diquark. Quarks of color 3, parallel to the condensate in color space, will be unaffected and propagate freely, with

$$S_0(p)^{bg}_{af} = i\delta^b_a\delta^g_f \left(\frac{\Lambda^+(p)}{p_o^2 - E_p^2} + \frac{\Lambda^-(p)}{p_o^2 - \bar{E}_p^2}\right)(p_\mu\gamma^\mu - \mu\gamma_0)\,. \tag{16}$$

This is written in terms of the particle and anti-particle projection operators $\Lambda^+(p)$ and $\Lambda^-(p)$, respectively, where $\Lambda^\pm(p) = (1 \pm \gamma_0\gamma\cdot\hat{p})/2$. The excitation energies are simply $E_p = |\mathbf{p}| - \mu$ for quarks and $E_p = |\mathbf{p}| + \mu$ for anti-quarks.

On the other hand, transverse quark colors 1 and 2 participate in the diquark and thus their quasi-particle propagators are given as

$$S(p)^{bg}_{af} = i\delta^b_a\delta^g_f \left(\frac{\Lambda^+(p)}{p_o^2 - \xi_p^2} + \frac{\Lambda^-(p)}{p_o^2 - \bar{\xi}_p^2}\right)(p_\mu\gamma^\mu - \mu\gamma_0)\,. \tag{17}$$

The quasi-particle energy is $\xi_p = \sqrt{(|\mathbf{p}| - \mu)^2 + \Delta^2}$, and for the anti-particle $\bar{\xi}_p = \sqrt{(|\mathbf{p}| + \mu)^2 + \Delta^2}$.

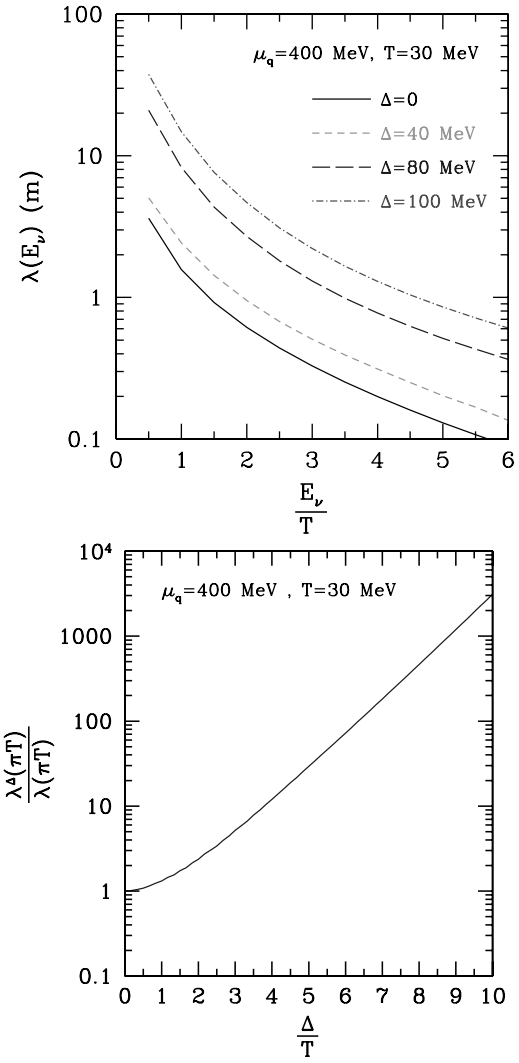

Fig. 3. Upper panel: neutrino mean free path as a function of neutrino energy E_ν. Lower panel: neutrino mean free path for $E_\nu = \pi T$ as a function of Δ/T. These results are virtually independent of temperature for $T \lesssim 50$ MeV.

The appearance of an anomalous propagator in the superconducting phase indicates that the polarization tensor gets contributions from both the normal quasi-particle propagators, eq. (17), and the anomalous propagator, eq. (15). Thus, to order G_F^2, eq. (13) is replaced with the two contributions corresponding to the normal and anomalous diagrams and is given by

$$\begin{aligned} \Pi_{\alpha\beta}(q) = -i\int \frac{\mathrm{d}^4p}{(2\pi)^4} \{&\mathrm{Tr}\,[S_0(p)\Gamma_\alpha S_0(p+q)\Gamma_\beta] \\ &+ 2\mathrm{Tr}\,[S(p)\Gamma_\alpha S(p+q)\Gamma_\beta] \\ &+ 2\mathrm{Tr}\,[F(p)\Gamma_\alpha \bar{F}(p+q)\Gamma_\beta]\}\,. \end{aligned} \tag{18}$$

The remaining trace is over spin, as the color trace has been performed.

For neutrino scattering we must consider vector, axial, and mixed vector-axial channels, all summed over flavors. The full polarization, to be used in evaluating eq. (1), may

be written as

$$\Pi_{\alpha\beta} = \sum_f \left[(C_V^f)^2 \Pi_{\alpha\beta}^V + (C_A^f)^2 \Pi_{\alpha\beta}^A - 2 C_V^f C_A^f \Pi_{\alpha\beta}^{VA} \right]. \quad (19)$$

The coupling constants for up-quarks are $C_V^u = \frac{1}{2} - \frac{4}{3}\sin^2\theta_W$ and $C_A^u = \frac{1}{2}$, and for down-quarks, $C_V^d = -\frac{1}{2} + \frac{2}{3}\sin^2\theta_W$ and $C_A^d = -\frac{1}{2}$, where $\sin^2\theta_W \simeq 0.23$ is the Weinberg angle.

The differential cross-section, eq. (1) and the total cross-section are obtained by integrating over all neutrino energy transfers and angles. Results for the neutrino mean free path, $\lambda = V/\sigma$, are shown in fig. 3 as a function of incoming-neutrino energy E_ν (for ambient conditions of $\mu_q = 400$ MeV and $T = 30$ MeV). They show the same energy dependence found previously for free relativistic and degenerate fermionic matter [12]; $\lambda \propto 1/E_\nu^2$ for $E_\nu \gg T$ and $\lambda \propto 1/E_\nu$ for $E_\nu \ll T$. The results indicate that this energy dependence is not modified by the presence of a gap when $\Delta \sim T$. Thus, the primary effect of the superconducting phase is a much larger mean free path. This is consistent with the suppression found in the vector-longitudinal response function, which dominates the polarization sum, eq. (19), at $q_0 < q$.

3.3 Neutrino interactions with Goldstone bosons

The discussion in the preceding section assumed that there were no low-energy collective excitations to which the neutrinos could couple. This is true in the 2-flavor superconducting phase of quark matter. For three flavors and when the strange-quark mass is negligible compared to the chemical potential, the ground state is characterized by pairing that involves all nine quarks in a pattern that locks flavor and color [25]. Naively, we can expect significant differences in the weak-interaction rates between the normal and the CFL phases of quark matter since the latter is characterized by a large gap in the quark excitation spectrum. However, diquark condensation in the CFL phase breaks both baryon number and chiral symmetries. The Goldstone bosons that arise as consequence introduce a low-lying collective excitations to the otherwise rigid state. Thus, unlike in the normal phase where quark excitations near the Fermi surface provide the dominant contribution to the weak-interaction rates, in the CFL phase, it is the dynamics of the low-energy collective states —the Goldstone bosons, that are relevant. Neutrino interactions with Goldstone bosons have been recently investigated by Jaikumar *et al.* [26] and Reddy *et al.* [27].

There are several articles that describe in detail the effective theory for Goldstone bosons in Color-Flavor–Locked quark matter [28]. We will not review them here except to note that it is possible to parameterize low-energy excitations about the $SU(3)$ symmetric CFL ground state in terms of the two fields $B = H/(\sqrt{24} f_H)$ and $\Sigma = e^{2i(\pi/f_\pi + \eta'/f_A)}$, representing the Goldstone bosons of broken baryon number H, and of broken chiral symmetry, the pseudo-scalar octet π, and the pseudo-Goldstone boson η', arising from broken approximate $U(1)_A$ symmetry.

The massless Goldstone boson associated with spontaneous breaking of $U(1)_B$ couples to the weak neutral current. This is because the weak isospin current contains a flavor singlet component. Although neutrinos couple to the flavor octet of Goldstone bosons, it turns out that the neutrino mean free path is mostly determined by processes involving the massless-baryon number Goldstone mode [27]. For this reason, we restrict our attention to these processes. The amplitude for the process involving the $U(1)_B$ Goldstone boson H and the neutrino neutral current is given by

$$A_{H\nu\bar{\nu}} = \frac{4}{\sqrt{3}}\, G_F\, f_H\, \tilde{p}_\mu\, j_Z^\mu\,, \quad (20)$$

where $\tilde{p}_\mu = (E, v^2\mathbf{p})$ is the modified four-momentum of the Goldstone boson and $v = 1/\sqrt{3}$ is the velocity of the Goldstone boson. The decay constant for the $U(1)_B$ Goldstone boson has also been computed in earlier work [28] and is given by $f_H^2 = 3\mu^2/(8\pi^2)$.

The neutrino mean free path due to the reaction $\nu \to H\nu$ can be calculated analytically and is given by

$$\frac{1}{\lambda_{\nu\to H\nu}(E_\nu)} = \frac{256}{45\pi} \left[\frac{v(1-v)^2(1+\frac{v}{4})}{(1+v)^2} \right] G_F^2\, f_H^2\, E_\nu^3. \quad (21)$$

Neutrinos of all energies can absorb a thermal meson and scatter into either a final-state neutrino by neutral current processes like $\nu + H \to \nu$ and $\nu + \pi^0 \to \nu$ or via the charged current reaction into a final-state electron by the process $\nu_e + \pi^- \to e^-$. These processes are temperature dependent as they are proportional to the density of mesons in the initial state. Mean free paths due to these processes, which we collectively refer to as Čerenkov absorption can be computed. Reactions involving the H-boson dominate over other Čerenkov absorption processes due to their larger population and stronger coupling to the neutral current. For this case, we find the neutrino mean free path is given by

$$\frac{1}{\lambda_{\nu H\to\nu}(E_\nu)} = \frac{128}{3\pi} \left[\frac{v\,(1+v)^2}{(1-v)} \right] \times \left[g_2(\gamma) + \frac{2v}{(1-v)} g_3(\gamma) - \frac{(1+v)}{(1-v)} g_4(\gamma) \right] \times G_F^2\, f_H^2\, E_\nu^3\,, \quad (22)$$

where $\gamma = 2vE_\nu/(1-v)T$ and the integrals $g_n(\gamma)$ are defined by the relation

$$g_n(\gamma) = \int_0^1 \mathrm{d}x\, \frac{x^n}{\exp(\gamma x) - 1}\,. \quad (23)$$

In contrast to processes involving the emission or absorption of mesons by neutrinos, the usual scattering process involves the coupling of the neutrino current to two mesons. As noted earlier, the amplitude for these processes vanishes for the H-meson and is suppressed by the factor p/f_π, where p is the meson momentum for the flavor octet mesons. Figure 4 shows the contribution of all

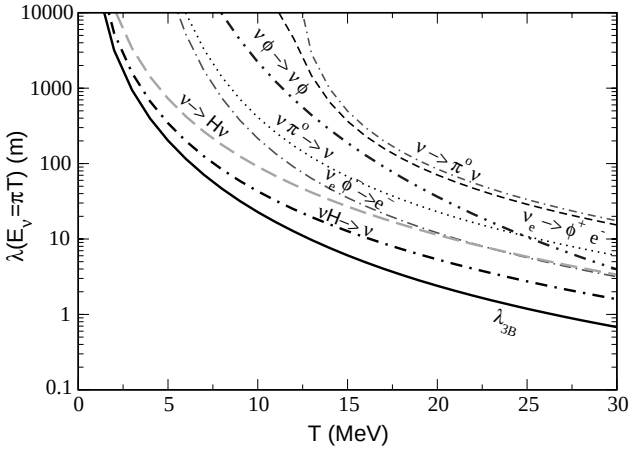

Fig. 4. Neutrino mean free path in a CFL meson plasma as a function of temperature. The neutrino energy $E_\nu = \pi T$ and is characteristic of a thermal neutrino.

Goldstone boson-neutrino processes contributing to the neutrino mean free path in the CFL phase including the dominant contribution arising from processes involving the massless mode.

It is interesting to note that the existence of one massless mode compensates for the large gap in the particle-hole excitations spectrum. The contrast between the findings of the previous section, wherein no low-energy Goldstone modes coupled to the neutrino, to those presented here is striking. The mean free path in the CFL phase is surprisingly similar to that in normal, non-superconducting, quark phase.

4 Discussion

We have attempted to provide a glimpse into the type of nuclear many-body calculations necessary to compute the response of dense matter to neutrinos. The methods employed and the fundamental questions being addressed have many similarities to those addressed in electron-nucleus scattering described at this meeting. While the latter approach probes the quark degrees of freedom inside nuclei by increasing the electron energy, the astrophysical setting allows us to probe similar questions using low-energy neutrinos.

Calculations of neutrino mean free paths and emission rates in dense matter remain a challenging problem to the nuclear many-body theorist. Several fundamental issues relating to the long-wavelength properties of the dense nucleonic matter and the role of phase transitions in neutron stars can be explored by employing these calculations in astrophysical simulations of neutron star phenomena.

I would like to thank Greg Carter, Jim Lattimer, Jose Pons, Madappa Prakash, Mariusz Sadzikowski and Motoi Tachibana for enjoyable collaborations. The material presented here are the fruits of these efforts. This work is supported in part by funds provided by the U.S. Department of Energy (D.O.E.) under cooperative research agreement DF-FC02-94ER40818.

References

1. M. Prakash, J.M. Lattimer, J.A. Pons, A.W. Steiner, S. Reddy, Lect. Notes Phys. **578**, 364 (2001).
2. R.F. Sawyer, Phys. Rev. D **11**, 2740 (1975).
3. B. Friman, O.V. Maxwell, Astrophys. J. **232**, 541 (1979).
4. N. Iwamoto, C.J. Pethick, Phys. Rev. D **25**, 313 (1982).
5. R.F. Sawyer, Phys. Rev. C **40**, 865 (1989).
6. C.J. Horowitz, K. Wehrberger, Nucl. Phys. A **531**, 665 (1991); Phys. Rev. Lett. **66**, 272 (1991); Phys. Lett. B **226**, 236 (1992).
7. G. Raffelt, D. Seckel, Phys. Rev. D **52**, 1780 (1995).
8. G. Sigl, Phys. Rev. Lett **76**, 2625 (1996).
9. S. Reddy, J. Pons, M. Prakash, M., J.M. Lattimer, in *Stellar Evolution, Stellar Explosions and Galactic Chemical Evolution*, edited by T. Mezzacappa (IOP Publishing, Bristol, 1997) p. 585.
10. S. Reddy, M. Prakash, Astrophys. J. **423**, 689 (1997).
11. M. Prakash, S. Reddy, in *Nuclear Astrophysics*, edited by M. Buballa, W. Nörenberg, J. Wambach, A. Wirzba (GSI, Darmstadt, 1997) p. 187.
12. S. Reddy, M. Prakash, J.M. Lattimer, Phys. Rev. D **58**, 013009 (1998).
13. S. Reddy, M. Prakash, J.M. Lattimer, J.A. Pons, Phys. Rev. C **59**, 2888 (1999).
14. A. Burrows, R.F. Sawyer, Phys. Rev. C **58**, 554 (1998).
15. A. Burrows, R.F. Sawyer, Phys. Rev. C **59**, 510 (1999).
16. C. Hanhart, D.R. Phillips, S. Reddy, Phys. Lett. B **499**, 9 (2001).
17. N.K. Glendenning, Phys. Rev. D **46** 4161 (1992).
18. S. Reddy, G.F. Bertsch, M. Prakash, Phys. Lett. B **475**, 1 (2000).
19. M. Christiansen, N.K. Glendenning, J. Schaffner-Bielich, Phys. Rev. C **62**, 025804 (2000); T. Norsen, S. Reddy, Phys. Rev. C **63**, 065804 (2001).
20. B.C. Barrois, Nucl. Phys. B **129**, 390 (1977); S.C. Frautschi, in *Proceedings of the Workshop on Hadronic Matter at Extreme Energy Density, Erice, Italy, 1978*, edited by N. Cabibbo, L. Sertorio (Plenum Press, New York, 1980).
21. M. Alford, K. Rajagopal, F. Wilczek, Phys. Lett. B **422**, 247 (1998); Nucl. Phys. B **357**, 443 (1999); **558**, 219 (1999); R. Rapp, T. Schäffer, E.V. Shuryak, M. Velkovsky, Phys. Rev. Lett. **81**, 53 (1998); Ann. Phys. (N.Y.) **280**, 35 (2000).
22. G.W. Carter, S. Reddy, Phys. Rev. D **62** 103002 (2000).
23. J. Bardeen, L.N. Cooper, J.R. Schrieffer, Phys. Rev. **108**, 1175 (1957).
24. R.D. Pisarski, D.H. Rischke, Phys. Rev. D **60**, 094013 (1999).
25. M.G. Alford, K. Rajagopal, F. Wilczek, Nucl. Phys. B **537**, 443 (1999).
26. P. Jaikumar, M. Prakash, T. Schafer, arXiv:astro-ph/0203088.
27. S. Reddy, M. Sadzikowski, M. Tachibana, arXiv:nucl-th/0203011.
28. R. Casalbuoni, R. Gatto, Phys. Lett. B **464**, 111 (1999); D.T. Son, M.A. Stephanov, Phys. Rev. D **61**, 074012 (2000); C. Manuel, M.H. Tytgat, Phys. Lett. B **479**, 190 (2000); S.R. Beane, P.F. Bedaque, M.J. Savage, Phys. Lett. B **483**, 131 (2000); T. Schafer, Phys. Rev. D **65**, 074006 (2002).